Recovery of Eroded Beach Seaward of Closed Katrina Cut in Dauphin Island, Alabama

Tingting Zhu[a,b,*] and Nobuhisa Kobayashi[a]

[a] *Center for Applied Coastal Research, University of Delaware, Newark, DE, USA*

[b] *Tianjin Research Institute for Water Transport Engineering, M.O.T., Tianjin, China*

[*] *Corresponding author: ztting@udel.edu*

ABSTRACT: A rubble mound structure was constructed in 2011 across the 2 km wide channel breached by Hurricane Katrina in 2005. The breached channel, known as Katrina Cut, is in Dauphin Island, Alabama. The recovery of the eroded beach seaward of the closed Katrina Cut was investigated using the numerical model CSHORE and data available between 2015 and 2020. The dry beach width increased more than 80 m seaward of the Katrina Cut structure and decreased up to 37 m on the neighboring beach. The computed onshore sand transport rate was large enough to cause the observed beach recovery. The empirical alongshore length associated with the longshore sand transport gradient was calibrated to predict the measured accretion and erosion pattern of the dry beach width. The recovering beach seaward of the structure reduced the depth-limited breaking wave height and wave action on the rubble mound structure during Hurricane Nate in 2017. This temporary structure helped recover the breached beach and may have become more lasting thanks to the increasing protection ensured by the front beach.

KEYWORDS: Shoreline accretion, sediment transport, barrier island, rubble mound, Hurricane Nate

1 INTRODUCTION

Barrier islands are common along the coasts in the Gulf of Mexico and provide a natural coastline protection. Morphological changes of barrier islands are mainly caused by sediment transport under normal daily waves and storm surges and waves. Hurricane Katrina produced a 2 km wide breach through the uninhabited beach segment of Dauphin Island, Alabama, in 2005 (Froede 2008). This breached channel called Katrina Cut (Fig. 1) was closed by a rubble mound structure constructed in 2011 (Webb et al. 2011). Beach recovery occurred seaward of the Katrina Cut structure with a visible increase in the dry beach width during 2011-2020 (Gonzalez et al. 2020). Mickey et al. (2020) assessed the decadal island evolution of Dauphin Island, and the response of seven different restoration measures devised as part of the Alabama Barrier Island Assessment to various storm and sea-level change scenarios using a long-term longshore sediment transport model, a short-term storm impact model, and an empirical dune growth model. Gonzalez et al. (2020) performed the structure response assessment of the Katrina Cut structure using a Monte Carlo life-cycle approach. The water depth in front of the structure was found to be im-

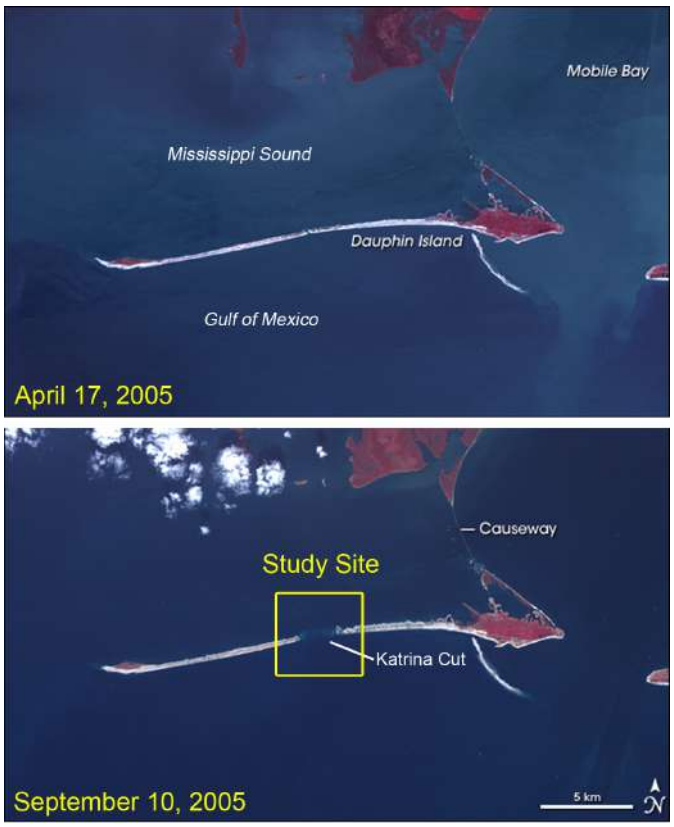

Figure 1: Location of the study site, Katrina Cut in Dauphin Island, Alabama (Imagery credited to Jesse Allen, NASA Earth Observatory).

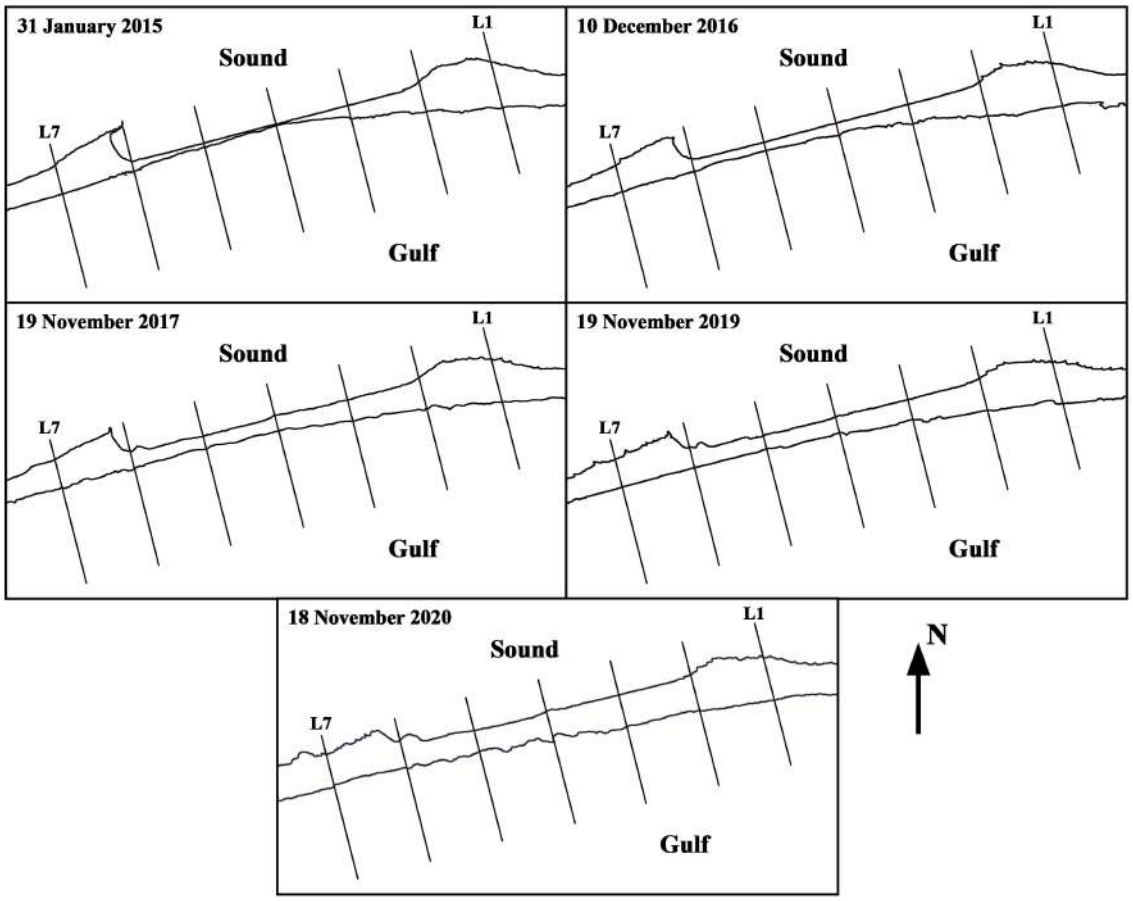

Figure 2: Shoreline contours in the vicinity of closed Katrina Cut in Dauphin Island, Alabama between the Gulf of Mexico and the Mississippi Sound from 2015 to 2020 and seven cross-shore lines (L1 – L7) oriented 16° counterclockwise from the north where the length of each line is 1 km.

portant in estimating breaking wave height. Coogan et al. (2019) measured subaerial geomorphic changes on Dauphin Island caused by overwash and inundation including regions near the Katrina Cut structure during Hurricane Nate in 2017. In this study, focuses are placed on long-term subaqueous sand transport processes and the breached beach recovery seaward of the Katrina Cut structure, as well as the effects of the recovering beach on structure stability. This study provides an example of the positive feedback between the structure and sediment.

Passeri et al. (2018) used a 2DH (two dimensional in the horizontal plane) XBeach model (Roelvink et al. 2009) to examine the influence of bed friction variability on the morphodynamics of the entire Dauphin Island during Hurricanes Ivan (2004) and Katrina (2005) before the construction of the Katrina Cut structure in 2011. The cross-shore model CSHORE (Kobayashi 2016) has been compared and verified with many small-scale and large-scale laboratory and field data of sand beach evolution and dune erosion. CSHORE is numerically efficient and was used to predict beach erosion and recovery along 16 cross-shore lines spanning 5 km alongshore for the duration of 272 days (Kobayashi and Jung 2012). CSHORE predicted both erosion and accretion above the mean sea level within a factor of about 2. The duration is extended to 2118 days in this study. CSHORE is also used to predict damage on the rubble mound by wave action.

2 AVAILABLE FIELD DATA

The shoreline positions of the closed Katrina Cut from 2015 to 2020 were analyzed using the topography of the five aerial images (Google Earth Pro) as listed in Table 1. The corresponding shoreline contours are depicted in Fig. 2. The Mississippi Sound and the Gulf of Mexico are located north and south of Dauphin Island. The dry beach seaward of the closed Katrina Cut became wider. The net longshore sand transport on the beach facing the Gulf of Mexico is to the west (e.g., Douglass 1994). The cross-shore profiles along lines L1-L7 of 1 km cross-shore length in Fig. 2 were extracted from the 2015 digital elevation model (DEM) with no restoration measure released by Mickey et al. (2019). The shoreline contour of January 31st 2015 in Fig. 2 is in agreement with the 2015 DEM shoreline based on the elevation $z = 0$ at the datum of NAVD88 (the North American Vertical Datum of 1988). Consequently, the shoreline contours of 31 January 2015 and the other four days in Fig. 2 are assumed to be located at the elevation $z = 0$ (NAVD88) in this study. The tide effect on the shoreline location is neglected for this micro-tidal beach, which has a mean tidal range of 0.36 m (NOAA 2021b). The fore-

Table 1: Dates of shoreline measurement and computation.

Time	Date	Number of Days
t_0	31 January 2015	0
t_1	31 December 2015	334
t_2	10 December 2016	679
t_3	19 November 2017	1023
t_4	30 November 2018	1399
t_5	19 November 2019	1753
t_6	18 November 2020	2118

shore slopes along L1-L7 were steeper than 1/15 (vertical/horizontal). The error of the shoreline location must be less than about 5 m. The alongshore distance between the two adjacent lines is 501.4 m.

The onshore coordinate x is taken as $x = 0$ at the seaward boundary in the water depth of about 6 m. The landward boundary of $x = 1,000$ m is located north of the Katrina Cut structure in the water depth of about 2 m. The alongshore coordinate y is positive toward the west. The shoreline contours facing the Gulf of Mexico are used to quantify the recovery of the eroded beach along L1-L7. The seaward displacement Δx of the shoreline from the shoreline location on 31 January 2015 is obtained as a function of the number of days since 31 January 2015. The dry beach width increased up to 83 m in front of the Katrina Cut structure (L2-L6) and decreased up to 37 m at the edges (L1 and L7) during the 2015-2020 period. Fig. 3 shows the seven initial profiles along the edge lines (L1, L2, L6, and L7) and the center lines (L3-L5) on 31 January 2015, respectively, where the onshore distance is zero at the shoreline location x_s of each line. The initial profiles of L3-L5 included a terrace near the elevation of -2 m. This terrace may have been the remnant bottom of the channel breached by Hurricane Katrina in 2005.

Douglass (1994) performed visual wave observations and beach profile surveys between 1990 and 1991 to investigate beach erosion and accretion as well as sediment transport paths along the Gulf of Mexico beaches of Dauphin Island. The sand is well sorted near the Katrina Cut and the median diameter is approximately 0.37 mm. The net longshore sand transport is westbound. The annual longshore sand transport rate is in the order of 10^5 m^3 per year. The average values of the monthly mean wave height, period, and angle near the Katrina Cut were about 0.6 m, 8 s, and 10°, respectively, where the wave angle is positive counterclockwise from the cross-shore line in Fig. 2. The positive wave angle results in positive longshore currents with sand being transported westwards. These data are used to select the representative waves and sediment for the following computations.

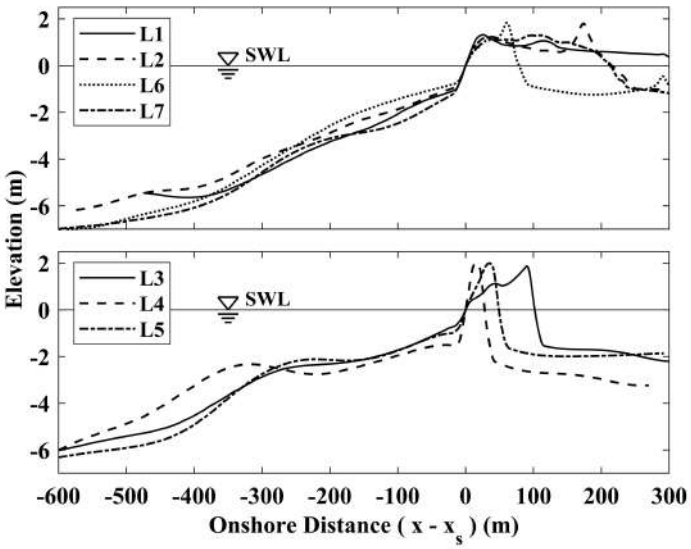

Figure 3: Seven initial profiles along the edge lines (L1, L2, L6, and L7) and the center lines (L3 – L5) as a function of onshore distance $(x - x_s)$ from the shoreline locations x_s of each line.

Table 2: Hurricanes with landfall date and peak water level recorded by tide gauge on Dauphin Island, Alabama.

Hurricane	Landfall Date	Peak Water Level (m)
Katrina	29 August 2005	1.75
Ida	10 November 2009	0.99
Isaac	29 August 2012	1.14
Nate	8 October 2017	1.17
Sally	15 September 2020	1.10
Zeta	29 October 2020	0.94

Tide gauge data at Dauphin Island (Tide Station 8735180) are available from the Center for Operational Oceanographic Products and Services at National Oceanic and Atmospheric Administration (NOAA 2021b). This tide station is located 13 km east of the study site. The mean high water, mean sea level, and mean low water based on the datum of NAVD88 are 0.207 m, 0.016 m, and -0.154 m, respectively. Offshore wave data was obtained from the National Data Buoy Center of NOAA (NOAA 2021a). The wave gauge (NDBC Buoy Station 42012) was located in the depth of 23.5 m off the coast of Orange Beach, AL (57 km east of the study site). The data was available during 1983-1984 and after 2009. The average values during 2015-2020 of the root-mean-square wave height H_{rms}, the spectral peak period T_p, and the peak spectral wave direction θ were 0.57 m, 5.4 s, and 6.2°, respectively. These values are reasonably similar to those observed by Douglass (1994). Major storm events since 2005 are reported in Table 2 together with the peak still-water elevation. The tide gauge data and wave data are used in the computation for Hurricane Nate in 2017 with the highest peak still-water level since 2009.

3 COMPUTATION OF ERODED BEACH RECOVERY

The dry beach width seaward of the rubble mound structure increased during 2015-2020 (Fig. 2). The

numerical model CSHORE is used to predict the observed beach recovery. The shoreline measurement dates are shown in Table 1. Two extra dates: 31 December 2015, and 30 November 2018, have been added to output the annual shoreline variation. For the sake of simplicity, we shall refer to t_0 = 0, t_1 = 334 d, t_2 = 679 d, t_3 = 1023 d, t_4 = 1399 d, t_5 = 1753 d, and t_6 = 2118 d. The initial beach profiles are extracted from the 2015 DEM data (Mickey et al. 2019) along the seven cross-shore lines (L1-L7). In this recovery computation, the buried rubble mound in 2015 is neglected because of the expected increase in dry beach width. The time series of H_{rms}, T_p, and θ need to be specified at the seaward boundary for a water depth of about 6 m. For this initial attempt to reproduce the long-term shoreline recovery, constant representative waves are assumed and taken as $H_{rms} = 0.6$ m, $T_p =$ 8 s, and $\theta = 10^\circ$ based on the visual observations by Douglass (1994). It was easier to detect numerical oscillations during the long-term (almost 6 years) computation under constant wave conditions. The sensitivity of the computed shoreline recovery to the assumed waves is presented in the next section. The still water level is assumed to be zero (NAVD88) for this micro-tidal beach. The median sand diameter is 0.37 mm. The specific gravity, porosity, and fall velocity of the sand are taken as 2.6, 0.4, and 0.051 m/s, respectively. The cross-shore nodal spacing is 2 m. The input parameters are taken as the standard values used in the previous beach erosion and recovery computations by Kobayashi and Jung (2012) who calibrated the bed load parameter $B = 0.001$ or 0.002. The computation time was 20 minutes for the computed duration of almost six years for each cross-shore line. The numerical efficiency of CSHORE allows for a number of calibration and sensitivity computations.

Fig. 4 shows the computed seaward shoreline displacement Δx using B = 0.001 and B = 0.002 as a function of the number of days for lines L1-L7 under the assumption of alongshore uniformity (IQYDY=0). The seaward shoreline displacement Δx is relative to the shoreline on 31 January 2015. The value of Δx is positive for shoreline accretion (shifting seaward) and negative for shoreline erosion (shifting landward). The decrease of the bed load parameter B reduces onshore sand transport and the seaward shoreline displacement. CSHORE predicts onshore bed load transport and offshore suspended load transport. The bed load transport rate is proportional to the value of B. Fig. 4 indicates the importance of onshore bed load transport in terms of beach recovery. In the following, B = 0.001 is adopted to reproduce the measured shoreline displacement.

The computed shoreline displacements for IQYDY=0 in Fig. 4 assume alongshore uniformity and do not account for the gradient of longshore sand transport. Two-dimensional horizonal models such as XBeach are available to simulate short-term bottom elevation changes. The bulged bathymetry in Fig. 3 is somewhat similar to a berm made of dredged sediment (e.g., McFall et al. 2021). Li (2021) presented such a model to predict the transport of placed dredged material in the surf and nearshore zones below the still water level (SWL) for the duration of about one month. The fronting beach elevation above the SWL affects the degree of damage to the rubble mound structure (Gonzalez et al. 2020). On the other hand, the long-term shoreline evolution has been predicted using a one-line model driven by longshore sediment transport in the zone between the closure depth and the berm height above the SWL. Ding et al. (2021) added cross-shore sediment transport to simulate shoreline changes for a 5 km shoreline over a 14-year period. The assumption of an active profile that translates in the direction of the cross-shore may be too crude for the bulged bathymetry in Fig. 3. CSHORE is adopted in this study because it predicts beach profile changes in the swash zone and in

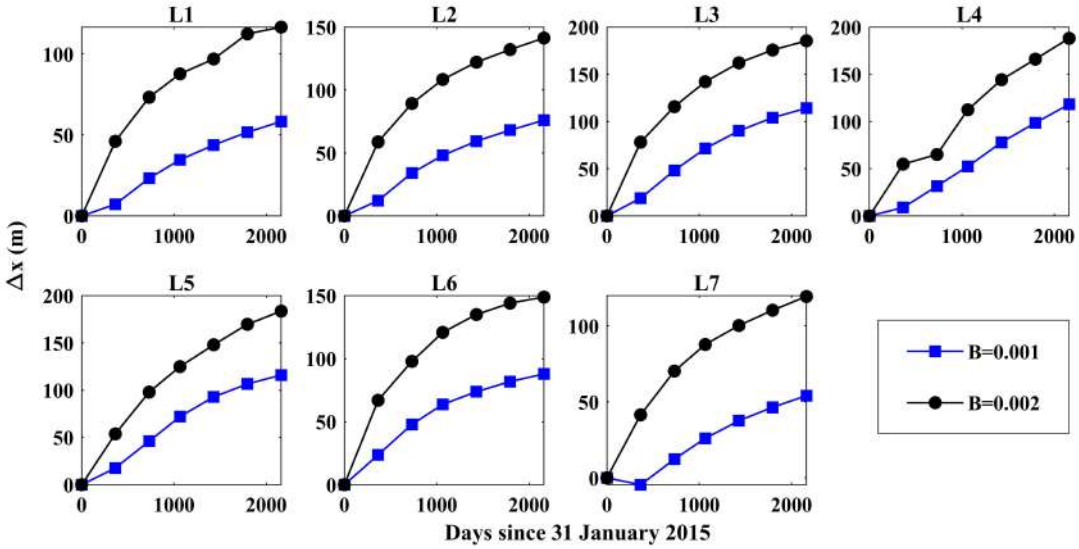

Figure 4: Computed seaward shoreline displacement Δx (m) as a function of the number of days since 31 January 2015 (Table 1) for lines L1 – L7 with Δx = 0 on zero day for bed load parameter B = 0.001 and 0.002.

the presence of a porous structure (Kobayashi and Kim 2017). The major shortcoming of CSHORE is the assumption of alongshore uniformity along each cross-shore line. Wave refraction and focusing over the bulged bathymetry are not included in the computation of irregular wave transformation. Zhu and Kobayashi (2021a) approximated the alongshore gradient of the longshore sediment transport rate per unit width, q_y, using the computed q_y on the given cross-shore line divided by the equivalent alongshore distance y_e, which was calibrated to account for alongshore sand loss or gain on the same cross-shore line. The computation for alongshore gradient in CSHORE is denoted by IQYDY=1. Integration of the approximate continuity equation from time t = 0 to an arbitrary value t yields

$$(1-n_p)[z_b(t,x,y)-z_b(t=0,x,y)]+\frac{\partial v_x}{\partial x}+\frac{v_y}{y_e}=0 \quad (1)$$

with

$$v_x=\int_0^t q_x dt; \quad v_y=\int_0^t q_y dt \quad (2)$$

where n_p = porosity of the bottom sediment, which is assumed as n_p = 0.4; z_b = bottom elevation (NAVD88); q_x = cross-shore total sediment transport rate (no void); and q_y = longshore total sediment transport rate (no void). The bottom elevation change at the given x and y in Eq. (1) depends on the spatial variations of the cross-shore volume v_x and longshore volume v_y per unit width. The alongshore length y_e in Eq. (1) rougly compensates for the effects neglected in the cross-shore model CSHORE and must be calibrated for each application. Inside the surf zone, the computed v_y is much larger than the computed v_x in Eq. (1). The cross-shore length scale of the cross-shore gradient in Eq. (1) is of the order of 100 m in Fig. 3. The alongshore length y_e is the longshore length scale and may be related to Katrina Cut width of about 2 km. The calibrated value is y_e = 1,000 m to mimic the observed alongshore variability of Δx among L1-L7.

The computed seaward shoreline displacements for IQYDY=0 and 1 at time $t = t_0 - t_6$ are compared with the measured shoreline displacement at time $t = t_0$, t_2, t_3, t_5, and t_6 for lines L1-L7 in Fig. 5. The computed Δx for IQYDY=0 and B = 0.001 is too large except for L4 in the middle of the Katrina Cut. The computed Δx for IQYDY=1 with the calibrated y_e is similar to the measured Δx. Eq. (1) implies the shoreline recovery due to onshore sand transport which is reduced by the positive westward longshore sand transport. It is also possible that the errors of v_x and v_y in Eq. (1) might have canceled out. The computed profile evolutions are examined to interpret the shoreline displacement depicted in Fig. 5.

Fig. 6 shows the initial profile and computed profiles for IQYDY=0 and 1 as well as the measured shoreline location (cross) at end time $t = t_6$ for L1-L7. The shoreline location is predicted better after the inclusion of the longshore sand transport term in Eq. (1). The bulged terrace near the elevation of -2 m (Fig. 3) is predicted to migrate landward under the computed onshore sand transport. Fig. 6 may indicate the importance of onshore sand transport for the recovery but no subaqueous profile data are available for the period after 2015. The computed step is located at the seaward edge of irregular wave breaking under the assumed constant water level and waves. This step may be artificial. Sand transported landward of the step is mostly deposited and shifts the shoreline seaward for L3-L5. Sand transported toward the shoreline along L1, L2, L6, and L7 is removed by longshore sand transport for the case of IQYDY=1.

The onshore sand transport volume (including void) per unit width is about 10 m^2/y at x = 0 in Fig. 6 and zero at the landward boundary x = 1,000 m. The computed rate at x = 0 is of the same order of magnitude as the computed rate by Kobayashi and Jung (2012) on Rehoboth and Dewey beaches in Delaware. The annual longshore sand (including void) transport rate Q_y (m^3/y) is computed for each cross-shore line. The cumulative longshore sand transport volume is obtained by integrating the longshore sand transport volume v_y per unit width from x = 0 to x = 1,000 m. The computed cumulative volume, as a function of time t, is divided by the duration t and converted to the annual rate Q_y which is consistent with the annual rate of the order of 10^5 m^3/y estimated by Douglass (1994). Byrnes et al. (2011) developed a regional sediment budget during 1917-2005 for Mississippi Sound barrier islands including Dauphin Island. The sand transport rate from the east to the west was about 3×10^5 m^3/y. The representative waves adopted for the shoreline change prediction may not be representative for the longshore sand transport rate. This uncertainty is absorbed in the calibrated y_e in Eq. (1).

4 SENSITIVITY OF COMPUTED RECOVERY TO REPRESENTATIVE WAVES AND SEDIMENT

The gross simplification of the representative waves for the shoreline recovery may be tolerable if the computed recovery is not very sensitive to the assumed constant waves. The computed results so far are limited to the incident waves represented by H_{rms} = 0.6 m, T_p = 8 s, and θ = 10°. The monthly average wave conditions near the study site presented by Douglass (1994) suggest the wave heights, periods, and angles in the ranges of 0.4 – 0.8 m, 6 – 10 s, and 5° – 15°, respectively. In the following, the computed shoreline displacements for three different values of H_{rms}, T_p, and θ are presented one by one. The sensitivity to the representative sediment diameter is discussed at the end. The computed shoreline displacements are limited to IQYDY=1 with y_e = 1,000 m.

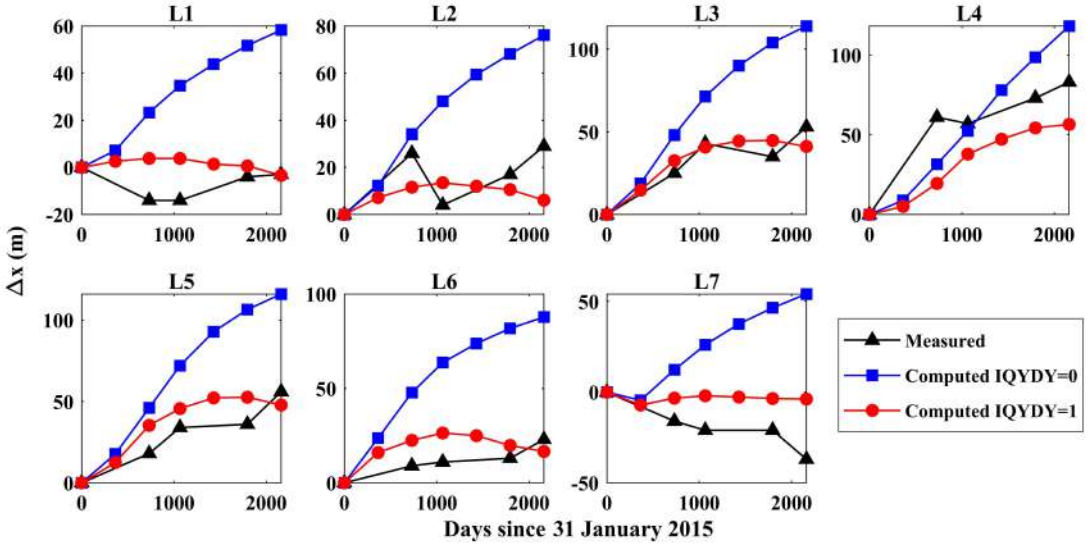

Figure 5: Computed shoreline displacement Δx (m) for alongshore uniform case (IQYDY=0) and alongshore gradient case (IQYDY=1 and y_e = 1,000 m) at time $t = t_0 - t_6$ for lines L1 – L7 as well as measured shoreline displacement at time $t = t_0$, t_2, t_3, t_5, and t_6 (Table 1).

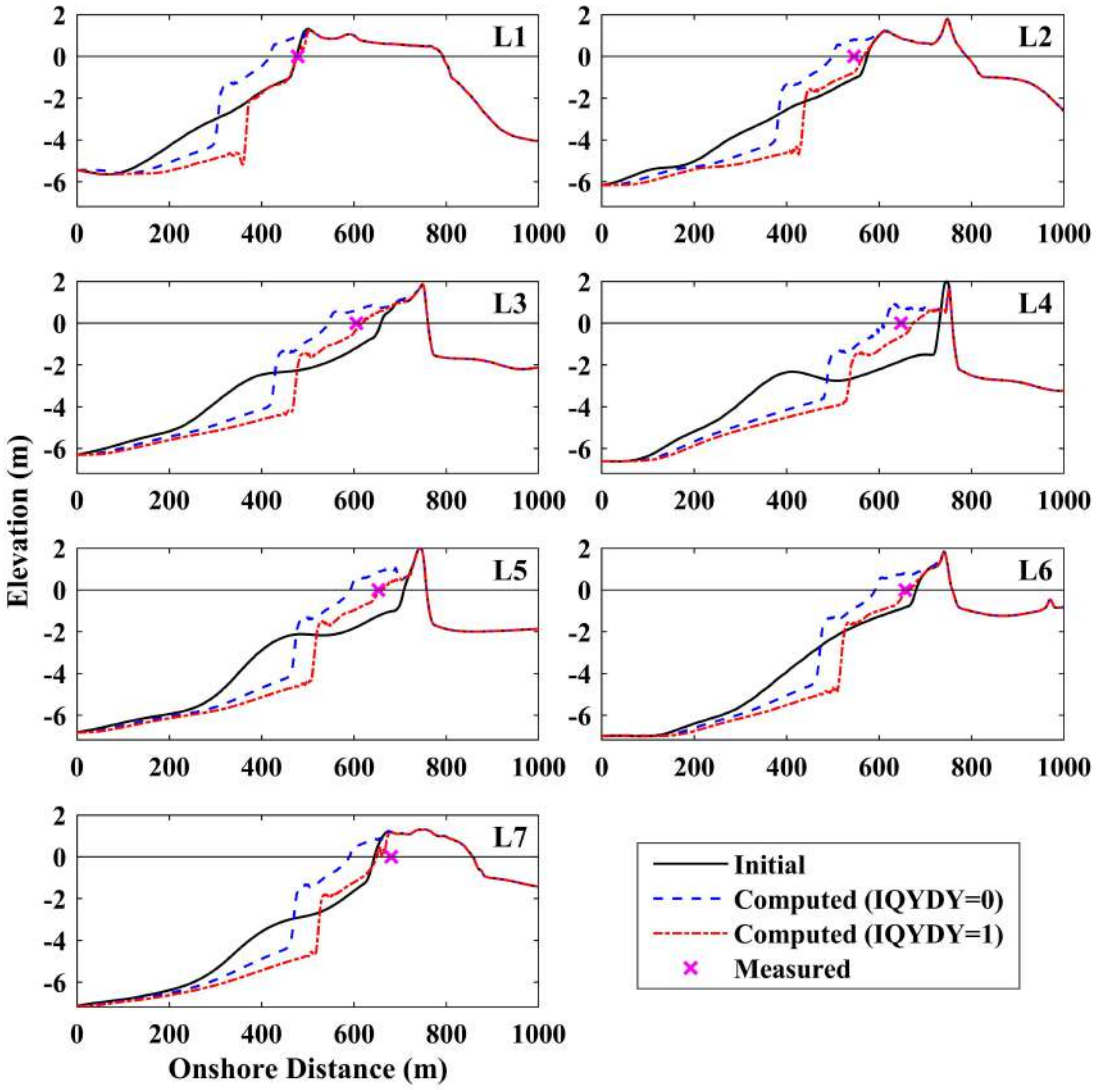

Figure 6: Initial and computed (IQYDY=0 and 1) profiles as well as measured shoreline location ($\times$) at end time $t = t_6$ for lines L1 – L7.

Fig. 7 shows the sensitivity to H_{rms} = 0.4, 0.6, and 0.8 m for T_p = 8 s and θ = 10°. The representative height H_{rms} = 0.6 m does not give the best agreement of all the seven lines. The agreement for L7 is the best for H_{rms} = 0.8 m. The agreement for L5 is slightly better for H_{rms} = 0.4 m. The computed shoreline displacement is accretional (positive) and roughly similar for H_{rms} = 0.4 and 0.6 m but can become erosional (negative) for H_{rms} = 0.8 m. The larger H_{rms} at the seaward boundary x = 0 increases the irregular breaking wave height, suspended sand volume per unit bottom area, and offshore suspended sand transport by undertow current in the surf zone (e.g., Kobayashi 2016). The accretional and erosional trends on this beach with the median sand diameter d_{50} = 0.37 mm are similar to those on the beaches in Delaware with d_{50} = 0.33 mm as computed by Kobayashi and Jung (2012). The average value of H_{rms} was 0.59 m for the accretional period of 221 days and 0.81 m for the erosional period of 51 days. Fig. 8 depicts the sensitivity to T_p = 6, 8, and 10 s for H_{rms} = 0.6 m and θ = 10°. The ranges of the computed values of Δx for the seven cross-shore lines (L1-L7) in Fig. 8 are less than the corresponding ranges in Fig. 7. The computed shoreline displacement is not very sensitive to the representative period T_p. No single value of T_p gives the best agreement for all the seven lines.

Fig. 9 shows the sensitivity to θ = 5°, 10°, and 15° for H_{rms} = 0.6 m and T_p = 8 s. The accretional shoreline displacement decreases with the increase of the wave angle θ because the longshore sand transport rate q_y increases as θ increases. For the case of IQYDY=1, the equivalent alongshore distance y_e has been calibrated as y_e = 1,000 m. The local bottom elevation change in Eq. (1) is determined by the cross-shore gradient of the cross-shore sediment transport volume v_x and the longshore volume v_y divided by y_e. This implies that the increase of v_y can be compensated by the increase of y_e. The calibrated value of y_e = 1,000 m is specifically for the representative waves of H_{rms} = 0.6 m, T_p = 8 s, and θ = 10°. Figs. 7 – 9 suggest that the uncertainties associated with the representative waves may produce 100% uncertainty of the computed shoreline displacement which is comparable with the 100% error of the sediment transport model in CSHORE (Kobayashi 2016). The use of representative waves is convenient for field sites with limited wave data, but the sensitivity to the assumed waves must be quantified for each application.

The sediment diameter d_{50} is 0.37 mm in the vicinity of the Katrina Cut and in the range of 0.28 – 0.43 mm on the beaches east of the Katrina Cut (Douglass 1994). Fig. 10 shows the sensitivity to d_{50} = 0.28, 0.37, and 0.43 mm for H_{rms} = 0.6 m, T_p = 8 s, and θ = 10°. The estimated fall velocities for the sand with d_{50} = 0.28, 0.37, and 0.43 mm are 0.036, 0.051, and 0.062 m/s, respectively. The computed accretional shoreline displacement Δx decreases for lower values of the sand diameter d_{50} except for L5 and d_{50} = 0.43 mm at time $t = t_2$ and t_3 (see Table 1). This is due to the increase of suspended sand volume and offshore suspended sand transport. For d_{50} = 0.28 mm, the values of Δx became negative (erosional) except for L4 with its initial shoreline on the rubble mound. The seaward shoreline displacement for L4 and d_{50} = 0.28 mm was zero because the rubble mound structure was not eroded. These sensitivity computations start from the initial profiles of L1-L7 in 2015 for d_{50} = 0.37 mm. The initial profiles for d_{50} = 0.28 and 0.43 mm could be different. Nevertheless, Fig. 10 indicates the importance of the sand diameter for the recovery of the eroded beach.

5 COMPUTATION FOR HURRICANE NATE

The effect of beach width on the rubble mound structure of Katrina Cut during Hurricane Nate is assessed for line L4 with the largest recovery of 83 m depicted

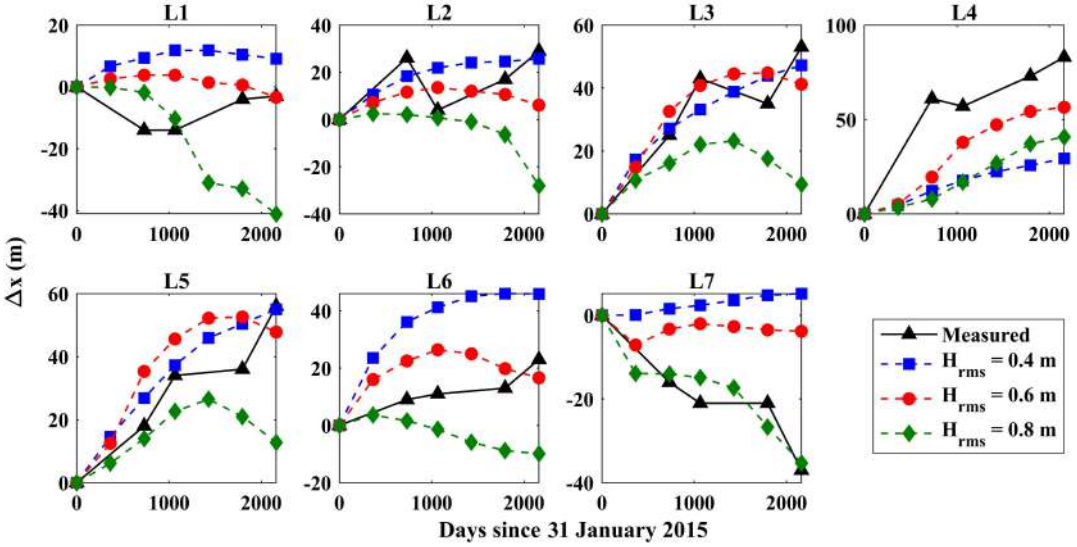

Figure 7: Computed shoreline displacement Δx (m) for root-mean-square wave height H_{rms} = 0.4, 0.6, and 0.8 m at time $t = t_0 - t_6$ for lines L1 – L7 as well as measured shoreline displacement where T_p = 8 s, θ = 10°, and IQYDY=1.

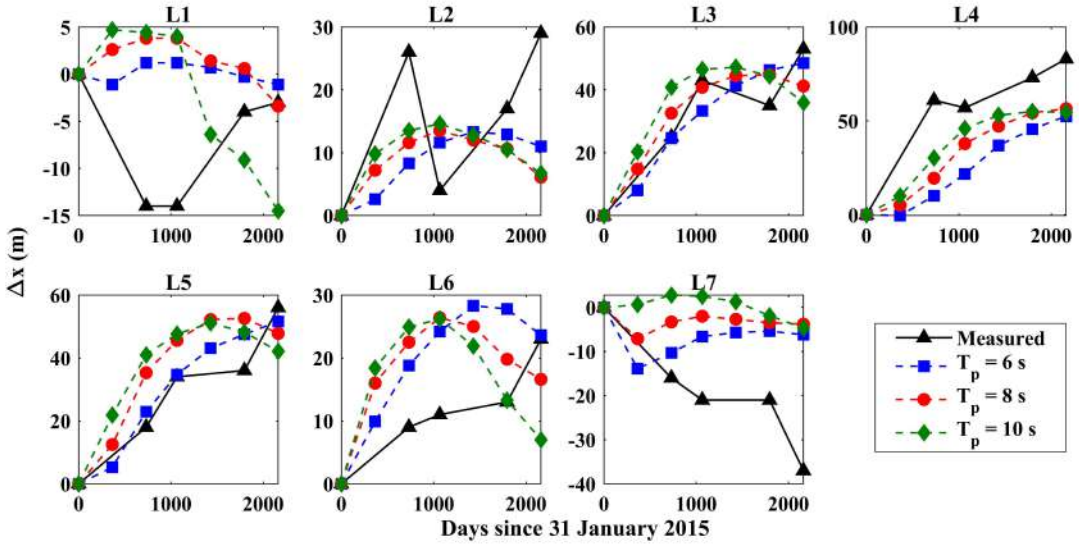

Figure 8: Computed shoreline displacement Δx (m) for spectral peak period T_p = 6, 8, and 10 s at time $t = t_0 - t_6$ for lines L1 – L7 as well as measured shoreline displacement where H_{rms} = 0.6 m, θ = 10°, and IQYDY=1.

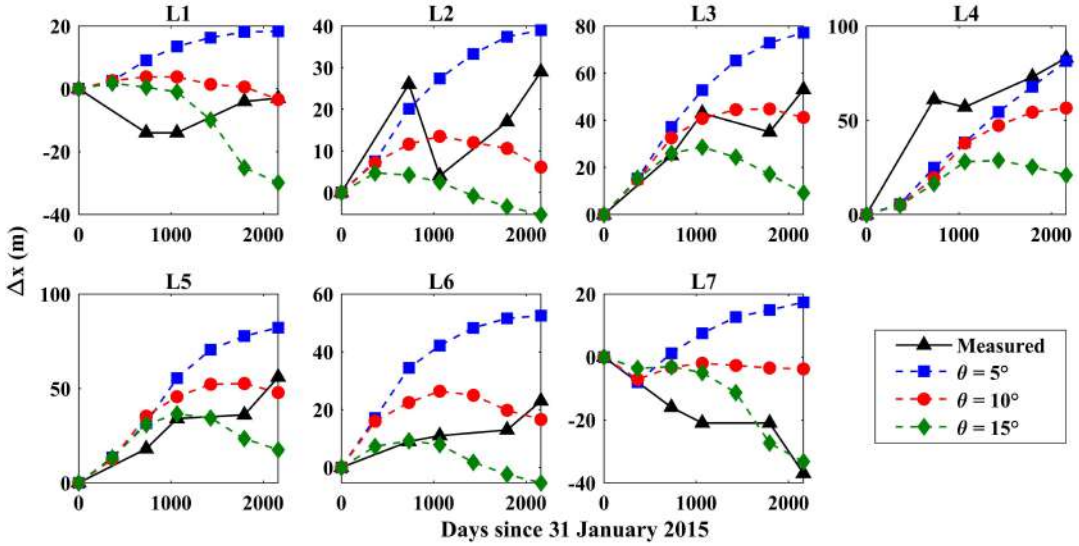

Figure 9: Computed shoreline displacement Δx (m) for peak spectral wave direction θ = 5°, 10°, and 15° at time $t = t_0 - t_6$ for lines L1 – L7 as well as measured shoreline displacement where H_{rms} = 0.6 m, T_p = 8 s, and IQYDY=1.

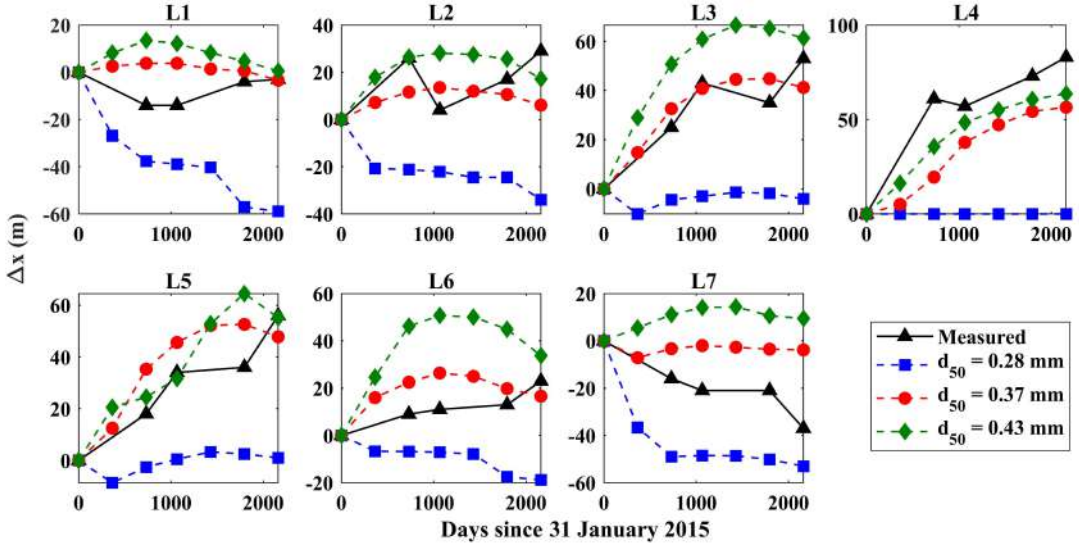

Figure 10: Computed shoreline displacement Δx (m) for sediment diameter d_{50} = 0.28, 0.37, and 0.43 mm at time $t = t_0 - t_6$ for lines L1 – L7 as well as measured shoreline displacement where H_{rms} = 0.6 m, T_p = 8 s, θ = 10°, and IQYDY=1.

in Fig. 6. The wave gauge located 57 km east of L4 is used to estimate the offshore waves at the water depth of 23.5 m. The computation domain of x = 0 – 1,000 m in Fig. 6 is extended offshore by 5,100 m by means of a bottom slope of 1/300 (vertical/horizontal). The new computation domain of x = 0 – 6,100 m starts from the water depth of 23.5 m at x = 0. The computed results near the Katrina Cut structure are essentially the same for the domain which has been extended by a 1/150-1/300 slope. The tide gauge located 13 km east of L4 is used to estimate the still water level. The waves near the shoreline are limited by depth-limited wave breaking. The time series of the still-water elevation, root-mean-square wave height H_{rms}, spectral peak period T_p, and wave angle θ shown in Fig. 11 are used as the seaward boundary conditions for line L4. The hourly time series started from 7 October 2017, one day before the landfall date of Hurricane Nate in Table 2. The time of the peak still-water level is indicated by a vertical line in Fig. 11. The computed results for IQYDY=0 and 1 were found to be almost the same, but the value of y_e is uncertain for Hurricane Nate. The computed results for IQYDY=0 (no y_e) are presented in the following.

The rubble mound structure with the seaward and landward slopes of 1/2 (vertical/horizontal) described by Gonzalez et al. (2020) is incorporated in the cross-shore beach profile along line L4 so that the structure could be exposed to wave action during Hurricane Nate. The crest and base widths of the rubble mound are 6.1 m and 22 m, respectively. The crest and toe elevations (NAVD88) are 2 m and -2 m, respectively. The nominal diameter, density, and porosity of the rock are 0.55 m, 2.6 g/cm^3, and 0.44, respectively. Four initial profiles along line L4 were investigated to examine the effect of recovering beach conditions on the rubble mound: (A) the hypothetical profile in 2011; (B) the surveyed profile in 2015; (C) the computed profile in 2017; and (D) the computed profile in 2020. The hypothetical profile in 2011 refers to the breached beach profile just after the structure construction obtained by removing sand above -2 m of the surveyed profile in 2015. The computed profiles are stored during the recovery simulation to obtain the 2017 profile on the starting day of Hurricane Nate and the 2020 profile at the end time t_6 (Fig. 6). The initial and final profiles at time t = 72 h of discernible profile change in the zone of x = 5,550 – 5,900 m are presented in Fig. 12 where the grey trapezoidal part is the cross-section of the rubble mound structure. The rock units are assumed to be stationary in this simulation of the beach profile change (Kobayashi and Kim 2017). No sand was present inside the 2011 rubble mound (A), whereas sand was assumed to cover the entire rubble mound in 2015 (B), 2017 (C), and 2020 (D). The 2011 profile mimicking the breached beach is predicted to be stable during the hurricane. Visible erosion is computed on the sand covered slope of the 2015 rubble mound. The eroded sand is predicted to be deposited on the fronting beach at the elevation near -2 m. For the 2017 and 2020 profiles with the recovered dry beach, the artificial step created by the representative waves is predicted to be eroded during the hurricane.

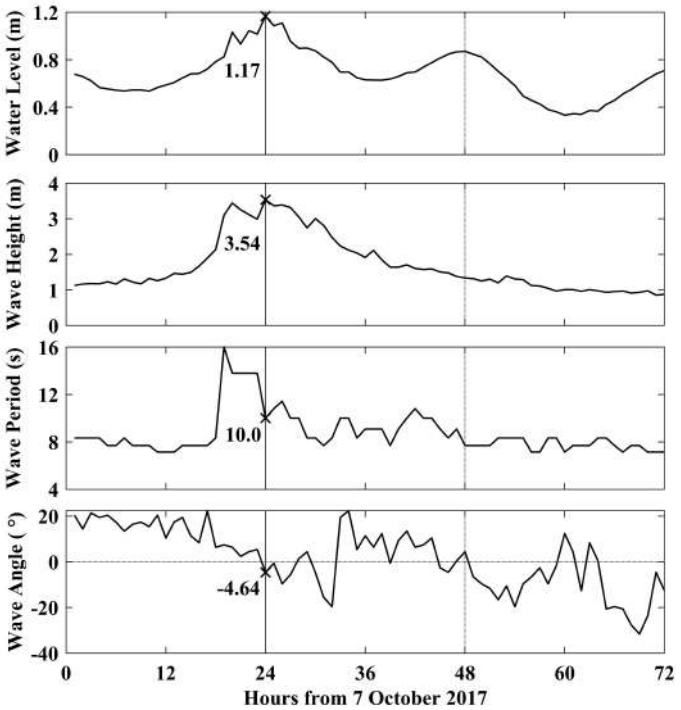

Figure 11: 3-day time series of still-water elevation at tide gauge and the wave height H_{rms}, peak period T_p, and angle θ at wave gauge during Hurricane Nate where the water level peaked on 8 October 2017 (Table 2).

Damage progression of a rubble mound structure during storms needs to be predicted for the structure design (Melby and Kobayashi 2011). The experiment by Zhu and Kobayashi (2021b) indicated little protection of a sand mound by a destroyed rock cover. The rubble mound deformation during Hurricane Nate is computed for the fixed initial beach profiles in Fig. 12. CSHORE cannot compute sand and rock movement simultaneously. No sand is assumed to exist inside the rubble mound above the fronting sand beach elevation so that armor rock units are exposed to direct wave action. Damage is defined as $S = A_e/(D_{n50})^2$ where A_e is the eroded armor area computed by CSHORE and D_{n50} is the nominal rock diameter of 0.55 m. The input critical stability number N_c for rock movement initiation is taken as 0.7 and 0.1 for careful and casual rock placement, respectively (Kobayashi et al. 2010; Yuksel and Kobayashi 2020). Fig. 13 shows the time variation of the calculated damage progression for the four cases in Fig. 12 during Hurricane Nate. The reduction of N_c from 0.7 to 0.1 causes increased damage for the 2011 and 2015 initial profiles (A and B). The 2016 visual observations by Gonzalez et al. (2020) suggested causal rock placement on this temporary structure. Damage progression is continuous for the most exposed case A in 2011 where the computed value of 3 for N_c = 0.1 at end time t = 72 h indicates cross-sectional damage of 3 rock units for the width of one rock diam-

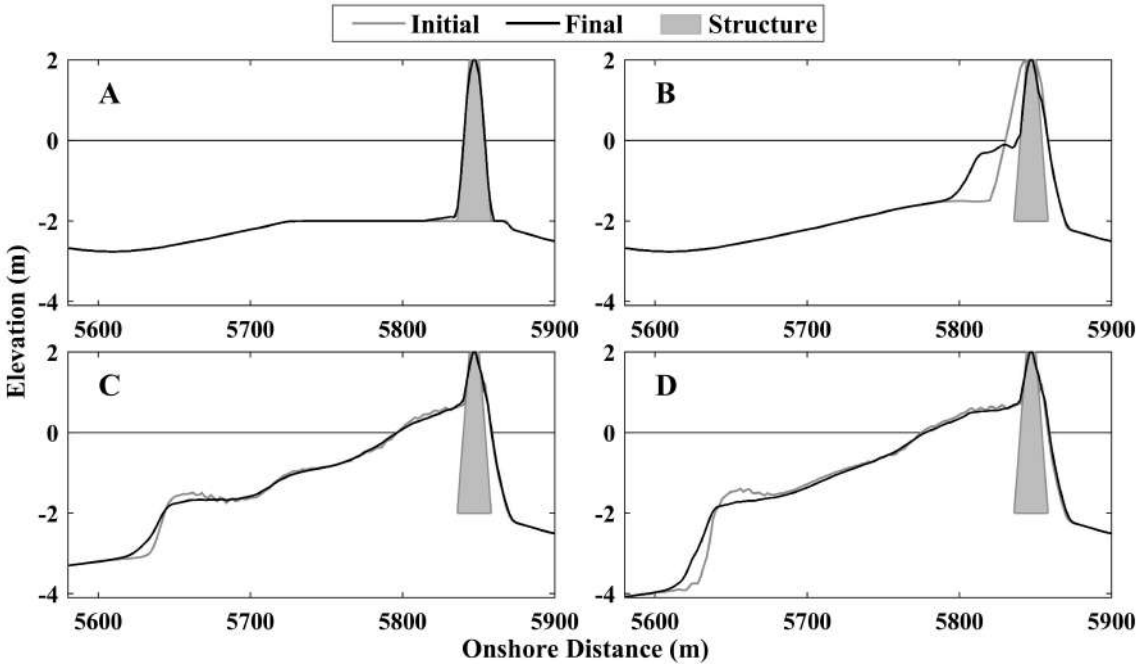

Figure 12: Initial profiles (A: hypothetical profile in 2011 after the rubble mound construction; B: measured profile in 2015; C: computed profile in 2017; D: computed profile in 2020) and computed final eroded profiles at the end of Hurricane Nate where the grey trapezoid indicates the rubble mound.

eter. For the less exposed case B in 2015, damage is computed to occur for seven hours near the peak still-water level at time t = 24 h (Fig. 11). For the 2017 and 2020 profiles with the fronting dry beach, the computed damage is practically zero even for N_c = 0.1. This is consistent with little structure damage to the infrastructure observed after Hurricane Nate in 2017 (Coogan et al. 2019). The damage differences calculated concern frontal beach elevations at -2.0 m, -1.5 m, 1.0 m and 1.0 m for the 2011, 2015, 2017 and 2020 profiles, respectively. The importance of the fronting beach elevation in reducing depth-limited breaking wave heights was stated by Gonzalez et al. (2020), who investigated how the beach affects structural stability. This involved an off-line linkage of the morphological models described in Mickey et al. (2020) based on a lifecycle structural response modeling approach.

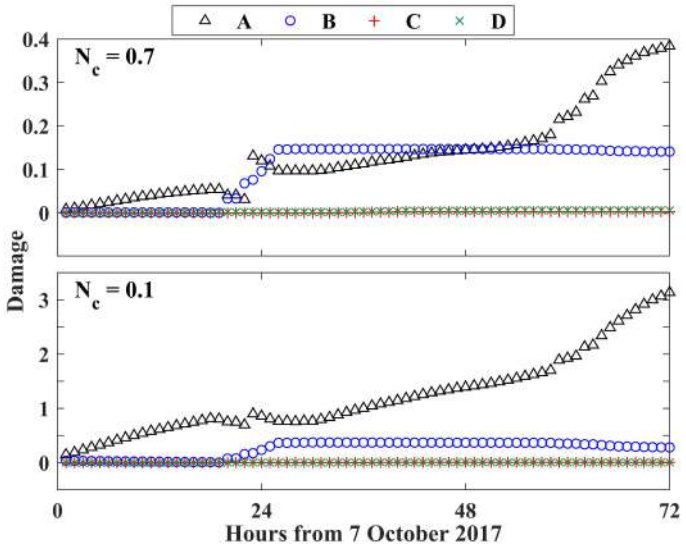

Figure 13: Computed damage of exposed armor rock layer above fronting sand beach during Hurricane Nate for critical stability number N_c = 0.7 and 0.1 corresponding to careful and casual rock placement, respectively, where the computed damage is almost the same for cases C and D in Fig. 11.

Kobayashi and Zhu (2017) developed a hypothetical Hurricane called SandyPlus. The still water level was increased to mimic that of a 500-year storm. This enabled the prediction of the impact of wave overtopping on a barrier beach. The same study also simulated a hypothetical storm called NatePlus.. The still water level in Fig. 11 was increased by 0.58 m for the entire 72-h duration to produce the peak water level of 1.75 m of Hurricane Katrina (Table 2), which caused the Katrina Cut. The offshore wave conditions and four initial profiles are kept the same. The critical stability number is N_c = 0.1. The computed profiles and damage progression for Hurricane NatePlus are compared with those of Hurricane Nate. The computed profile changes (Fig. 12) increase somewhat in the vicinity of the rubble mound. The computed damage for the 2011 and 2015 profiles is larger but the damage increment is less than about 1.2. The computed damage for the 2017 and 2020 profiles remains small and is less than about 0.2. The water level increase of 0.58 m is predicted to increase the beach erosion and armor damage but the predicted increase is relatively minor, perhaps because of the Katrina Cut structure constructed in 2011 after Hurricane Katrina in 2005.

6 CONCLUSIONS

The rubble mound structure constructed in 2011 to close the breach in Dauphin Island caused by Hurricane Katrina in 2005 was investigated along seven

cross-shore lines between 2015 and 2020 (almost a six-year period) using the numerical model CSHORE. Constant representative waves are proposed to reproduce the recovering dry beach width seaward of the rubble mound structure. Onshore sand transport on the breached beach restores the dry beach width, and longshore sand transport moves sand alongshore. However, the 500-metre alongshore distance between the seven cross-shore lines meant that they were too sparse to estimate the alongshore gradient of the longshore sediment transport rate. The empirical alongshore length was calibrated to reproduce the alongshore variation of the dry beach width changes with time because the assumption of local alongshore uniformity in CSHORE was too crude for the bulged bathymetry of the breached beach in this study. The sensitivity of the beach recovery to the assumed representative waves is examined to quantify the expected error of this convenient engineering approach. The estimated error of 100% is similar to the error of the sediment transport model in CSHORE. Furthermore, the recovery of the eroded beach is sensitive to the sand diameter.

The long-term recovery computation did not include the rubble mound structure and storm conditions. The beach profile changes and the rubble mound damage during Hurricane Nate lasting 3 days were computed for the cross-shore line of the largest recovery. The survey profile in 2015 and three possible profiles in 2011, 2017, and 2020 were used as the initial profiles. The erosional profile changes during the stormy 3 days were much smaller than the accretional profile changes under the constant waves lasting almost six years. The computed armor layer damage during Hurricane Nate in 2017 was negligibly small for the 2017 and 2020 beach profiles with the recovering wide beach. The computed damage became noticeable for the 2015 profile with a narrow dry beach and exceeded 3 rock units for the width of one rock diameter for the hypothetical 2011 profile just after the rubble mound was constructed. The construction of the Katrina Cut structure aided natural sand transport recovery processes. In return, the recovering beach dissipates storm waves and reduces wave action on the structure. The sensitivity computations using CSHORE suggest that this mutual aid may occur under certain wave, sediment, and structure conditions. New data are necessary to confirm the findings in this study.

ACKNOWLEDGMENTS

This work was supported by the U.S. Coastal Research Program under Agreement No. W912HZ-20-2-0016.

REFERENCES

Byrnes, M. R., J. D. Rosati, & S. F. Griffee (2011). Sediment budget: Mississippi Sound barrier islands. In *Proceedings of the Coastal Sediments 2011: In 3 Volumes*, pp. 2366–2379. World Scientific.

Coogan, J. S., B. M. Webb, S. M. Smallegan, & J. A. Puleo (2019). Geomorphic changes measured on Dauphin Island, AL, during Hurricane Nate. *Shore & Beach 87*(4), 15–22.

Ding, Y., R. Styles, S. C. Kim, R. L. Permenter, & A. E. Frey (2021). Cross-shore sediment transport for modeling long-term shoreline evolution. *Journal of Waterway, Port, Coastal, and Ocean Engineering 147*(4), 04021014.

Douglass, S. L. (1994). Beach erosion and deposition on Dauphin Island, Alabama, USA. *Journal of Coastal Research 10*(2), 306–328.

Froede, C. R. (2008). Changes to Dauphin Island, Alabama, brought about by Hurricane Katrina (August 29, 2005). *Journal of Coastal Research 24*(4C), 110–117.

Gonzalez, V. M., F. A. Garcia-Moreno, J. A. Melby, N. C. Nadal-Caraballo, & E. S. Godsey (2020). Alabama Barrier Island Restoration Assessment lifecycle structure response modeling. Technical Report ERDC/CHL TR-20-5, U.S. Army Engineer Research and Development Center, Coastal and Hydraulics Laboratory, Vicksburg, MS.

Kobayashi, N. (2016). Coastal sediment transport modeling for engineering applications. *Journal of Waterway, Port, Coastal, and Ocean Engineering 142*(6), 03116001.

Kobayashi, N., A. Farhadzadeh, & J. A. Melby (2010). Wave overtopping and damage progression of stone armor layer. *Journal of waterway, port, coastal, and ocean engineering 136*(5), 257–265.

Kobayashi, N. & H. Jung (2012). Beach erosion and recovery. *Journal of waterway, port, coastal, and ocean engineering 138*(6), 473–483.

Kobayashi, N. & H. D. Kim (2017). Rock seawall in the swash zone to reduce wave overtopping and overwash of a sand beach. *Journal of Waterway, Port, Coastal, and Ocean Engineering 143*(6), 04017033.

Kobayashi, N. & T. Zhu (2017). Bay flooding through tidal inlet and by wave overtopping of barrier beach. *Journal of Waterway, Port, Coastal, and Ocean Engineering 143*(5), 04017024.

Li, H. (2021). Transport of placed dredged material in surf and nearshore zone. *Journal of Waterway, Port, Coastal, and Ocean Engineering 147*(3), 05021002.

McFall, B. C., K. E. Brutsché, A. M. Priestas, & D. R. Krafft (2021). Evaluation techniques for the beneficial use of dredged sediment placed in the nearshore. *Journal of Waterway, Port, Coastal, and Ocean Engineering 147*(5), 04021016.

Melby, J. A. & N. Kobayashi (2011). Stone armor damage initiation and progression based on the maximum wave momentum flux. *Journal of Coastal Research 27*(1), 110–119.

Mickey, R. C., E. Godsey, P. S. Dalyander, V. Gonzalez, R. L. Jenkins III, J. W. Long, D. M. Thompson, & N. G. Plant (2020). Application of decadal modeling approach to forecast barrier island evolution, Dauphin Island, Alabama. Technical Report 2020-1001, US Department of the Interior,U.S. Geological Survey.

Mickey, R. C., R. L. Jenkins III, P. S. Dalyander, D. M. Thompson, N. G. Plant, & J. W. Long (2019). Dauphin Island decadal forecast evolution model inputs and results. U.S. Geological Survey data release, `https://doi.org/10.5066/P9PDM1OJ`.

National Oceanic and Atmospheric and Administration (NOAA) (2021a). National Data Buoy Center - 42012 Orange Beach, 44 NW SW of Mobile, AL. `https://www.ndbc.noaa.gov`. [Online; last accessed October 2021].

National Oceanic and Atmospheric and Administration (NOAA) (2021b). Tides & Currents - Water Levels - 8735180 Dauphin Island, AL. `https://tidesandcurrents.noaa.gov`. [Online; last accessed October 2021].

Passeri, D. L., J. W. Long, N. G. Plant, M. V. Bilskie, & S. C. Hagen (2018). The influence of bed friction variability due to land cover on storm-driven barrier island morphodynamics. *Coastal Engineering 132*, 82–94.

Roelvink, D., A. Reniers, A. Van Dongeren, J. V. T. De Vries, R. McCall, & J. Lescinski (2009). Modelling storm impacts on beaches, dunes and barrier islands. *Coastal engineering 56*, 1133–1152.

Webb, B. M., S. L. Douglass, C. R. Dixon, & B. Buhring (2011). Coast guards. *Civil Engineering Magazine 81*(12), 76–83.

Yuksel, Z. T. & N. Kobayashi (2020). Comparison of revetment and sill in reducing shore erosion and wave overtopping. *Journal of Waterway, Port, Coastal, and Ocean Engineering 146*(1), 04019028.

Zhu, T. & N. Kobayashi (2021a). Modeling of soft cliff erosion by oblique breaking waves during a storm. *Journal of Waterway, Port, Coastal, and Ocean Engineering 147*(4), 04021009.

Zhu, T. & N. Kobayashi (2021b). Rock mound to reduce wave overwash and crest lowering of a sand barrier. *Coastal Engineering Journal 63*(4), 504–516.